A novel method for approximating local changes in the surface absorption for laser marking using 3D laser scanning

Mikkelstrup, Anders Faarbæk; Thomsen, Anders Noel; Kristiansen, Morten

Published in:
IOP Conference Series: Materials Science and Engineering

DOI (link to publication from Publisher):
10.1088/1757-899X/1135/1/012002

Publication date:
2021

Document Version
Publisher's PDF, also known as Version of record

A novel method for approximating local changes in the surface absorption for laser marking using 3D laser scanning

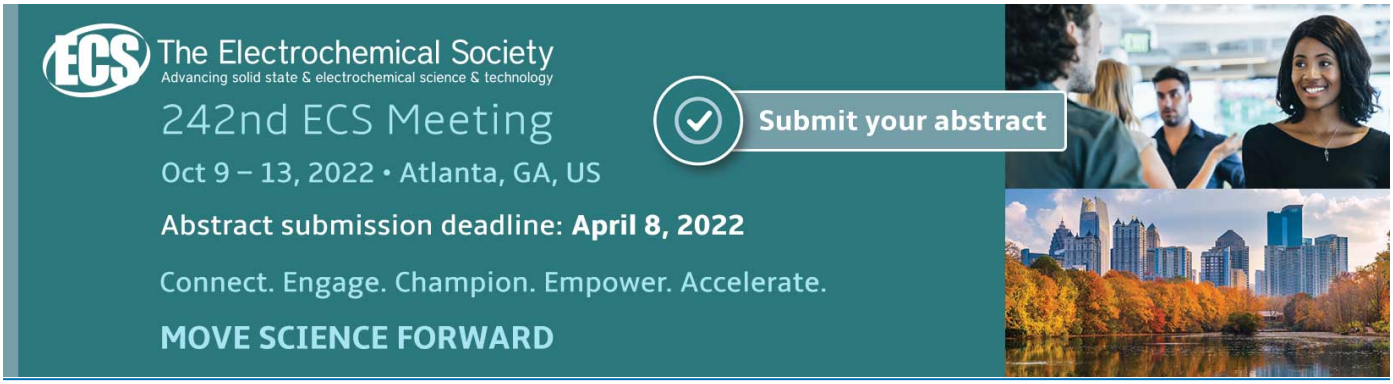

IOP Conf. Series: Materials Science and Engineering 1135 (2021) 012002 doi:10.1088/1757-899X/1135/1/012002

A novel method for approximating local changes in the surface absorption for laser marking using 3D laser scanning

Anders F. Mikkelstrup[1], Anders N. Thomsen[1], Morten Kristiansen[1]

[1]Department of Materials and Production, Aalborg University, Fibigerstraede 16, 9220 Aalborg East, Denmark

afm@mp.aau.dk

Abstract. Laser marking is a non-contact technique, which achieves colouring by using a laser beam to increase surface oxidation. Controlling the amount of heat induced into the part is essential in ensuring the desired degree of oxidisation. However, the induced heat is not only dependent on the process parameters, but also on the surface absorption, which in turn is dependent on the material, laser wavelength, and surface quality, i.e., current degree of oxidation and contaminants as well as surface roughness. This paper proposes a method for correlating backscatter from a 3D laser scanner with the surface absorption of sheet metal parts. The purpose is to determine local changes in the surface absorption caused by surface oxidation and contamination. The method utilises a 3D laser scanner, which projects a laser line at the surface and measures the resulting backscatter at an angle. The proposed solution applies a bi-directional reflectance model to reduce the influence of varying scanning angles. The method's sensitivity to variations in surface treatments is investigated and validated against backscatter spectroscopy measurements. The results show that the proposed method can identify changes in the absorption. However, these were, in some cases, more than 70% higher compared to spectroscopy measurements.

1. Introduction

Laser marking is a method for increasing the thickness of the oxide layer by increasing the temperature. By changing the thickness, light is refracted differently, which gives colour changes. This can be used for aesthetic and communicative purposes in parts of metal. Controlling the colouring is a matter of process settings [1] and surface properties. The surface absorption describes the energy coupling efficiency of the surface. It thus is defined as the ratio between the incident energy from the laser and the absorbed energy by the surface [2]. As laser marking is dependent on controlling the induced heat into the material, knowledge of the absorption plays an essential role in the process stability and quality. It is well known that surface absorption is influenced by contamination, oxidation and roughness. Typically, surface contamination of sheet metal components originates from fingerprints and oil residue from manufacturing. Oxidation arises from oxygen reacting with the surface and will for stainless steel present itself as a thin layer of chromium oxide. The oxidation process will naturally occur over time but can be expedited by inducing heat, which is the principle behind laser marking. Abedi and

Hoseinpour [3] found that by coating the surface of an AISI 304L sample with an oxide layer, the surface absorption of wavelengths exceeding 1000 nm could be more than doubled.

Roughening the surface of the sample showed comparable results. Niu et al. [4] and Bergström et al. [5] discovered that the surface morphology and surface structure drastically influences the absorption, especially at incident angles below 60° in which a rougher surface generally leads to an increase in the absorption. Niu et al. [4] further concluded that the effect of the incident angle is dependent on the structure of the surface. However, the impact of the incident angle generally becomes less prominent as the surface roughness is increased. Moreover, the polarisation of the laser and the type of laser is known to affect the correlation between the incident angle and the absorption [6]. In addition, Niu et al. [4] investigated the influence of the laser wavelength in the spectrum from 0.4 μm to 4 μm and concluded that the absorption generally decreases with increasing wavelength.

The surface absorption in the solid state of a material can be estimated through a number of theoretical methods and indirect and direct measurement techniques [7]. Theoretical approaches like the classic Drude model [8] and Hagen and Rubens [9] rely on knowledge of parameters such as surface roughness, oxidation, contamination, and material properties.

Indirect measurement techniques are based on computational models to estimate the surface absorption. These methods take into account parameters such as the surface roughness [10], beam intensity [11], angle of incidence [12] and surface temperature [13]. As a result, they generally offer an improved estimation of the surface absorption compared to the purely theoretical methods.

The direct measurement techniques are both accurate and straightforward experimental methods, which can be split into two groups: Methods that directly measure the absorption (calorimetry methods [14]) and methods that indirectly measure the absorption by the radiative properties of the surface, e.g., reflectance and emission (radiometric methods) [7,15]. However, calorimetry methods cannot provide a local estimation of the surface absorption compared to methods that indirectly measure the absorption by the radiative properties of the surface, such as reflectometry and emittance spectroscopy. Kügler and Vollertsen [16] used an integrated sphere to perform reflectometry spectroscopy to determine the absorption of stainless steel. The experimental set-up consisted of a 300 mW laser diode with a wavelength of 1030 nm, which was utilised to radiate the sample, while a Si-photodiode captured the reflected radiation. The integrated sphere spectrophotometry provides simple and highly accurate measurements. Though, as each sample must be placed inside the integrated sphere, it is not sustainable in a flexible production set-up and is further limited in the physical size of the sample.

A range of theoretical models, indirect and direct measurement techniques have been developed for estimating absorption. However, none can provide a local estimation of the absorption for use in a flexible laser marking set-up. As a result, it becomes challenging to locally control the induced heat into the material, which, as mentioned earlier, is a prerequisite for laser marking to obtain a stable process and quality.

The literature review indicates a need for a solution that can determine local changes in the absorption in a flexible manufacturing step-up. The main contribution of this paper is to investigate the feasibility of using a 3D laser scanner to provide an approximation of the absorption as a preceding step for laser marking of stainless steel. By correlating the backscatter from a 3D laser scanner, it is possible to approximate local changes in the surface reflectivity. As the surface reflection is highly dependent on incident angle and perspective, the received backscatter intensity is corrected based on the Cook-Torrance bi-directional surface reflectance (BRDF) model. A series of laser marking experiments are performed to oxidate the surface and create varying levels of reflectivity across the surface of the part to validate the developed method. The results are further compared with the measured values from spectroscopy. The remainder of the paper is organised as follows: In Section 2, the experimental set-up for laser marking and geometrical and intensity measurements is presented. In Section 3, the developed method for correcting intensity values and identifying areas with increased or decreased surface reflectivity is shown. In Section 4, the results are presented and discussed. Section 5 includes the concluding remarks of the paper.

2. Experimental set-up

The experimental set-up is presented in Figure 1 and Figure 2, which, respectively, illustrates laser processing and geometrical and reflectivity measurements of a part. The laser processing set-up consists of a 3 kW IPG YLS-3000 SM laser connected to a modified HighYag processing head. The focal length is 470 mm with a collimated beam diameter of 11.05 mm. The beam quality is 1.2 M^2 with a wavelength of 1076 nm. The measurement set-up consists of a Wenglor MLWL153 3D line scanner, which is applied to acquire a 3D surface representation of the processed parts. The scanner uses a class 3R laser beam with a wavelength of 407 nm and a CMOS sensor to determine the position of the projected laser. The CMOS sensor can further measure the backscatter intensity from the projected laser in a 10-bit greyscale resolution.

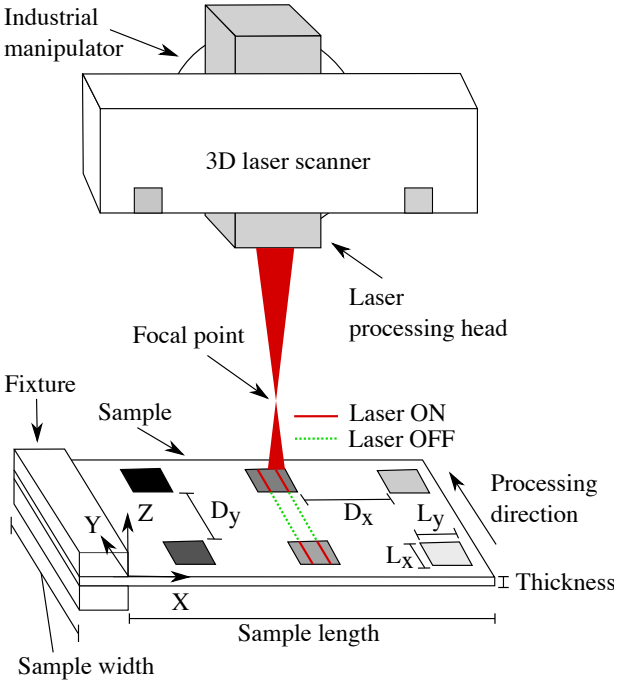

Figure 1. Laser processing set-up for laser marking.

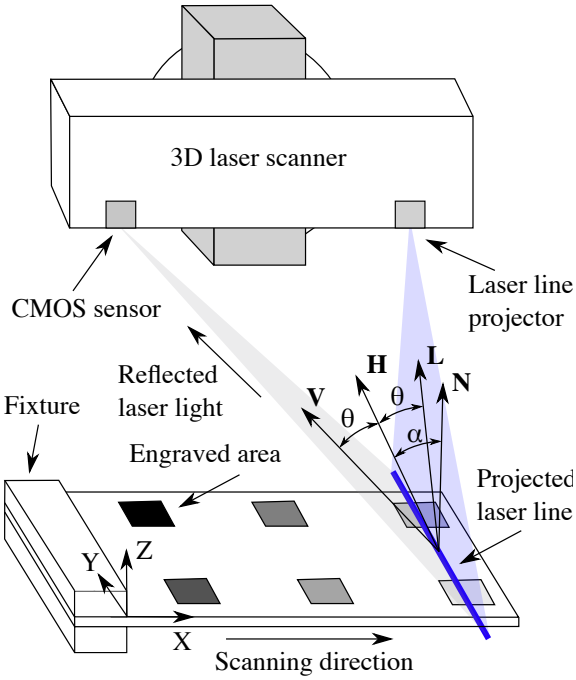

Figure 2. Measurement set-up for geometrical and intensity measurements. The projected laser line is observed by the CMOS sensor at a varying angle depending on the distance to the measured surface.

It should be noted that the specifications of both the laser and the optical components in the scanner are not disclosed by the manufacturer and, therefore, unknown to the authors. The processing head and the 3D line scanner are mounted onto and manipulated by a KUKA KR120 R2700 industrial robot for accurate and flexible positional control. Additionally, spectroscopy measurements have been performed using a LAMBDA 1050+ UV/Vis/NIR spectrophotometer with an integrated sphere to capture diffuse and specular reflectance at normal incidence. Each measured reflectivity is taken as an average of three measurements with a spacing of approximately 5 mm apart. The measured spot size was 3 x 3 mm.

The experiments consisted of three main phases: laser marking, laser scanning and spectroscopy. Spectroscopy and 3D scanning were done preceding laser marking to establish a set of reference values. Subsequently, laser marking was performed on the samples at varying speeds and power levels to generate different oxidation levels and different surface reflections. Finally, spectroscopy was performed again, along with 3D scanning of the samples. Table 1 states the parameters used for laser marking and 3D scanning, while Table 2 includes an overview of the experimental samples. The area # of Table 1 refers to the processed/engraved area, as illustrated in figures 2 and 3.

Table 1. Overview of samples for laser marking and reflectance measurements.

Area #	Scanning speed [mm/min]	Power [W]	Pulse frequency [Hz]	Duty cycle [%]	Spot size [mm]	Overlap [%]	3D scanning speed [mm/min]	3D scanning exposure time [ns]
1	7000	2300	5000	11	1	80	15000	400
2	7300	2300	5000	11	1	80	15000	400
3	7000	2100	5000	11	1	80	15000	400
4	7300	2100	5000	11	1	80	15000	400

Table 2. Overview of samples for laser marking and reflectance measurements. All samples are of rolled AISI 304L stainless steel plates.

Sample #	Treatment	Size [mm x mm x mm]	Reflection [%] λ = 407 nm	Reflection [%] λ = 1076 nm
1	Untreated	100 x 100 x 2	48.60	58.84
2	Untreated	100 x 100 x 2	48.65	62.83
3	Treated with WD-40	100 x 100 x 2	35.77	46.65
4	Treated with WD-40	100 x 100 x 2	37.90	49.65
5	Ground P80 – linear pattern	100 x 100 x 2	53.28	62.68
6	Ground P80 – random pattern	100 x 100 x 2	51.44	60.52

3. Method

The proposed method is based on measuring backscatter from a 3D scanner to locally approximate changes in the reflectivity of the laser light from the 3D scanner. The 3D scanner uses laser triangulation principles, which rely on geometric relations between the projected beam and the CMOS in the scanner. As the beam is projected in an opposite V-shape from the scanner onto the surface, the incident angle of the beam changes across the scanning width (Y-direction of Figure 2). For a perfect diffuse or Lambertian surface, the reflected light is scattered homogenously into the hemisphere, and the surface will hence appear equally bright regardless of the observed perspective. Lambert's cosine law defines a directly proportional relationship between the cosine of the incident angle and surface normal and the amount of reflected light in the given direction. Thus, it is apparent from Lambert's law that the measured backscatter intensity will not be constant across a flat surface. However, perfectly diffuse surfaces are rare in practice, as the majority of surfaces compose of an additional specular component that represents light being concentrated around the mirror direction. This is especially problematic when scanning reflective surfaces, i.e., rolled steel and other metals, as light can be reflected directedly into the sensor, resulting in high local backscatter intensities.

The ratio between the diffuse and specular components of reflected light depends on the optical properties of the surface, i.e. surface roughness and material composition [17]. The remainder of light that is not reflected will either be transmitted or absorbed by the material, hence equation (1):

$$I_i = I_d + I_s + I_a + I_t \tag{1}$$

I_i is the radiance of incident light, I_d is the diffused radiance, I_s is the specular radiance, I_a is the absorbed radiance, and I_t is the transmitted radiance, which for opaque materials like steel is typically zero. Hence, the absorbed radiance I_a can be approximated by determining I_i, I_d and I_s.

The 3D scanner is utilised to acquire 3D geometrical data of the surface and the corresponding backscatter intensities at each point in the shape of a point cloud. The reflection characteristics of the surface can be determined by modelling the specular and diffusion reflection using a bi-directional reflectance model (BRDF). The result is a rendered surface, which will act as a reference for determining changes in reflectivity across the actual surface. This approach aims to correct the received backscatter intensities and minimise the geometrical effects resulting from changes in incident angles. The Cook-

Torrance model, proposed by Cook and Torrance [18], is a BRDF based on optics theory and is well suited for rendering metallic surfaces. Furthermore, it can be generalised for numerous surfaces and represent both diffuse and specular reflections. Other mathematically simpler BRDF models are only able to represent diffuse surfaces (Oren-Nayer [19]) or have been shown not to be realistic enough for applicability (Blinn-Phong [20]). The Cook-Torrance model is further physically plausible, meaning that it obeys the laws of energy conservation and the Helmholtz Reciprocity. It should, however, be noted that the Cook-Torrance model assumes that the light is unpolarised and that the surface is isotropic, which can be a problematic assumption when dealing with ground surfaces. Reflection from other objects is also not considered. As stated by Cook and Torrance [18], the bi-directional reflectance can be expressed as the ratio between the reflected intensity from one direction and the incident radiance from another direction. Hence, the reflected intensity is given by equation (2):

$$R = \frac{I_r}{I_i(\mathbf{N} \cdot \mathbf{L})\mathrm{d}\omega_i} \tag{2}$$

Where I_r is the reflected intensity, I_i is the incident radiance, while $\mathrm{d}\omega_\mathrm{i}$ is the differential solid angle of the light source i. $\mathbf{N}$ is the surface normal, and $\mathbf{L}$ is the unit vector in the direction of the incident light, as illustrated in Figure 2. The Cook-Torrance BRDF represents the reflection as the sum of the diffuse R_d and specular R_s reflection, controlled by the material-dependent specular s and diffuse d fractions as given by equation (3).

$$R = sR_s + dR_d, \qquad \text{where } s + d = 1 \tag{3}$$

Based on equation (2), the intensity reflected into the sensor I_r is then given by equation (4).

$$I_r = RI_i(\boldsymbol{N} \cdot \boldsymbol{L})\mathrm{d}\omega_i \tag{4}$$

By introducing the ambient light term I_a and its corresponding reflectivity R_a, the intensity of the reflected light I_r can be expressed as the sum of the ambient term and the sum of the contribution from each light source. The ambient term consists of light that is not directedly pointed at the surface. In this case, the laser from the 3D scanner is represented as a number of individual light sources with small solid angles $\mathrm{d}\omega_\mathrm{i}$, which combined make up the entire width of the projected beam. To reduce computational complexity, it is assumed that each light source l only radiates the single point (or pixel of the rendered surface) that it hits. In this case, the reflectance intensity I_r is not computed over the entire hemisphere and thus only represents the reflection from a single point I_p in a single direction (direction of the CMOS sensor). I_p is then expressed in equation (5).

$$I_p = I_{ia}R_a + I_{il}(\boldsymbol{N} \cdot \boldsymbol{L_l})\mathrm{d}\omega_{il}(sR_s + dR_d) \tag{5}$$

Computing I_p for all points in the acquired point cloud from the 3D scanner will result in a $1 \times n$ vector that can be rearranged into a matrix form to be represented as a 2D rendered image of the surface reflection.

The specular reflection R_s can be expressed by combining the Fresnel term, the facet slope distribution D and the shadowing-masking term G, as given by equation (6).

$$R_s = \frac{F}{4}\frac{DG}{(\boldsymbol{N} \cdot \boldsymbol{L})(\boldsymbol{N} \cdot \boldsymbol{V})} \tag{6}$$

$\mathbf{V}$ is the unit vector in the direction of the observer, which in this case is the CMOS sensor in the scanner. The Fresnel term F introduces wavelength dependence to the model and expresses the reflectance of a perfectly smooth surface based on the index of refraction n. For most metals, the index

of refraction has experimentally been determined and can be found in the literature [21]. The Fresnel term is approximated using the cheaper Schlick approximation [22], given by equation (7).

$$F = F_0 + (1 - F_0)[1 - (\mathbf{L} \cdot \mathbf{H})]^5, \qquad \text{where } F_0 = \left(\frac{1-n}{1+n}\right) \tag{7}$$

The diffuse reflection R_d is assumed to be of the same colour as the specular reflection R_s and is therefore expressed as $\underline{R_d} = F_0/\pi$. Assuming that the ambient light is uniformly incident on the surface, the ambient reflectivity can be defined as $R_a = \pi R_d$. Assuming that the surface consists of a distribution of microfacets D that only reflect specular light, the angular spread of the specular component s can be determined. It should be noted that it is merely micro facets whose normal are in the direction of the normalised bi-sector vector $\mathbf{H}$ that contribute to the observed specular reflection. $\mathbf{H}$ is defined such that $\cos(\theta) = \mathbf{V} \cdot \mathbf{H} = \mathbf{L} \cdot \mathbf{H}$, where θ is the angle between $\mathbf{V}$ and $\mathbf{H}$ or $\mathbf{L}$ and $\mathbf{H}$, as illustrated in Figure 2. As given by equation (8), the Beckman distribution considers the root mean square (RMS) of the facet slopes σ and is based on Gaussian roughness assumptions. The Beckman distribution is the commonly preferred distribution in the literature [23].

$$D(\mathbf{N}) = \frac{1}{\pi\sigma^2(\mathbf{N} \cdot \mathbf{H})^4} \exp\left[\frac{-\tan^2(\alpha)}{\sigma^2}\right], \qquad \text{where } \alpha = \cos^{-1}(\mathbf{H} \cdot \mathbf{N}) \tag{8}$$

Small values of σ represent a relatively smooth surface, resulting in a highly directional specular component, while higher values of σ represent steep facet slopes and, therefore, a rougher surface. The shadowing-masking term G describes the probability of a microfacet being visible in the ingoing (shadowing) and outgoing (masking) and is thus angular dependent [24]. Walter et al. [23] recommend using the Smith approximation, equation (9), as it serves as a more realistic representation compared to the term initially proposed by Cook and Torrance [18].

$$G_1(\mathbf{V}, \mathbf{H}) = \chi^+\left(\frac{\mathbf{V} \cdot \mathbf{H}}{\mathbf{V} \cdot \mathbf{N}}\right) \begin{cases} \dfrac{3.535y + 2.181y^2}{1 + 2.276y + 2.577y^2} & \text{if } y < 1.6, \\ 1 & \text{otherwise} \end{cases} \tag{9}$$

Where $y = (\sigma \tan \langle \mathbf{V}, \mathbf{N} \rangle)^{-1}$ and $\langle \mathbf{V}, \mathbf{N} \rangle$ is the angle between the unit vectors $\mathbf{N}$ and $\mathbf{V}$. As the Smith G approximation is a product between the two monodirectional shadowing terms G_1, G is given by equation (10).

$$G(\mathbf{L}, \mathbf{V}, \mathbf{H}) \approx G_1(\mathbf{L}, \mathbf{H}) \cdot G_1(\mathbf{V}, \mathbf{H}) \tag{10}$$

The unit vectors $\mathbf{N}$, $\mathbf{H}$, $\mathbf{V}$ and $\mathbf{L}$ are acquired from the 3D geometrical data from the point cloud. As the laser specifications from the 3D scanner are unknown to the authors, it is impossible to directly compute the intensity of the incident light I_i. The RMS value of the facet slope σ of the surface is equally an unknown parameter. The same applies to the intensity of the ambient light I_a and the specular and diffuse fractions s and d. The diffuse fraction d can be computed based on equation (3), hence $d = s - 1$. The RMS facet slope σ, the fraction of specular light s and the intensity of the incident and ambient light, respectively I_i and I_a, are determined through a non-linear least square problem by minimising the difference between the computed reflectance intensities I_p and the acquired backscatter intensities I_b from the 3D scan. The fitted parameters (σ, s, I_i, I_a) are then applied to generate a perfect reference surface W_r free from any local changes in reflection due to surface contamination or oxidation. A rendered surface is illustrated in Figure 3 (left).

The acquired backscatter intensities I_b from the 3D scanner, Figure 3 (right), is reshaped as a matrix W_b and then compared to the generated reference surface W_r. This results in the relative change in

reflectivity (or light intensity) ΔR, given by equation (11). ΔR is illustrated as an image in Figure 3 (right).

$$\Delta R = \frac{W_r}{W_b} \cdot 100 \tag{11}$$

As it is challenging to accurately determine surface absorption values, it is chosen to approximate the relative change in reflectivity ΔR. As it is clear from equation (1), the reflectivity is directly related to the absorption. By assuming that no light is transmitted through the material, a change in the surface reflection corresponds to a change in the surface absorption.

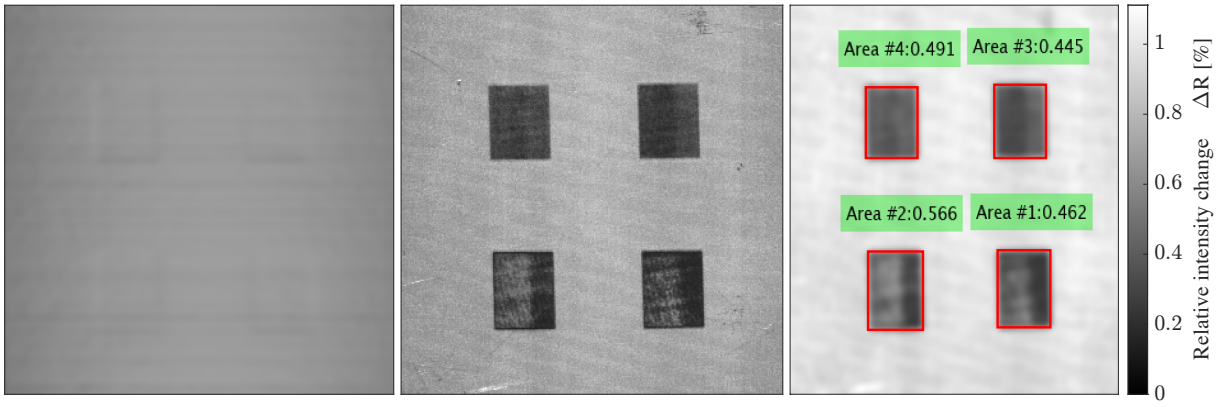

Figure 3. Left: Rendered image W_r of the surface of Sample 3 based on the Cook-Torrance BRDF model. Centre: Intensity backscatter surface W_b acquired by the 3D scanner of Sample 3. Note that the processed areas have a decreased ΔR, observed as the darker areas. Right: An image based on relative intensity change ΔR between the rendered surface W_i and the backscatter intensities W_b. Note that the values on the figure are the average ΔR within each red rectangular outline.

4. Results and discussion

The estimated relative change in reflectivity ΔR of all samples across selected, processed areas is compared with ΔR values obtained through spectroscopy. The reference values used to compute ΔR for the spectroscopy measurements is the reflectivity of the given sample before processing. Table 3 presents an overview of the measured ΔR using both the 3D scanner, spectroscopy at λ = 405 nm and λ = 1076 nm. Due to limited resources with the spectrophotometer, only samples 2 and 3 have been measured in all processed areas.

Table 3. Overview of relative change in reflectivity ΔR obtained from the 3D scanner and spectroscopy

	ΔR 3D scanning [%]				ΔR Spectroscopy [%], λ = 405 nm				ΔR Spectroscopy [%], λ = 1076 nm			
Area #	# 1	# 2	# 3	# 4	# 1	# 2	# 3	# 4	# 1	# 2	# 3	# 4
Sample 1	34	45.9	40.8	44.5		37.6		26.1		81.6		96.1
Sample 2	33.9	44.1	45	48.2	32.3	25.6	26.9	30.7	86.8	90.5	98	99.1
Sample 3	46.2	56.6	44.5	49.1	55.6	45.6	32.8	39.1	103.2	99.4	122.3	123.4
Sample 4	42.3	50.8	47.5	49.1		52.8		35.9		98.2		117.4
Sample 5	43.7	48.6	32.4	39.4		38.9		34.1		76.3		94.7
Sample 6	26.6	60.6	44.2	56.2		37.2		30.9		81.1		95.4

Table 4 presents a percentage comparison of the determined ΔR values from Table 3 based on the relation presented in equation (12).

$$C = \frac{\Delta R_{scan} - \Delta R_{spectroscopy}}{\Delta R_{spectroscopy}} \cdot 100\ \% \tag{12}$$

Table 4. 3D scanning versus spectroscopy. Percentage comparison of ΔR.

	C Spectroscopy [%], λ = 405 nm				C Spectroscopy [%], λ = 1076 nm			
Area #	# 1	# 2	# 3	# 4	# 1	# 2	# 3	# 4
Sample 2	4.95	72.27	67.29	57	-62.79	-71.71	-72.5	-51.36
Sample 3	-16.91	56.6	35.67	36.78	-55.23	-44.06	-63.61	-58.18

The results of tables 3 and 4 show that the proposed solution can identify changes in the reflection. However, there is generally a significant deviation (in some cases > 70%) in the measured ΔR values compared to spectroscopy. As isotropy is assumed in the model, a deviation is expected in the ground samples 4 and 5. The deviation is further expected to be substantial when comparing ΔR from the 3D scanner to those obtained by spectroscopy at λ = 1076 nm due to the difference in the wavelength. Therefore, the application of the proposed method should be made using a measuring laser that has a wavelength closer to that of the applied processing laser to minimise approximation error. Another source of error could be due to the presented laser marking experiments being conducted on standard industrial AISI 304L sheet metal to resemble a real industrial manufacturing scenario. This induced that the surface of the samples was not entirely homogeneous, which produces a visible variation in the absorption and thereby the marking results, as seen in Figure 4 (left). This effect was evident compared to the results presented by Antończak et al. [1] conducted on well-prepared surfaces. As the spectroscopy measurements are performed in an area of 3 x 3 mm, there is additionally a possible risk of accidentally measuring an area with considerably higher absorption.

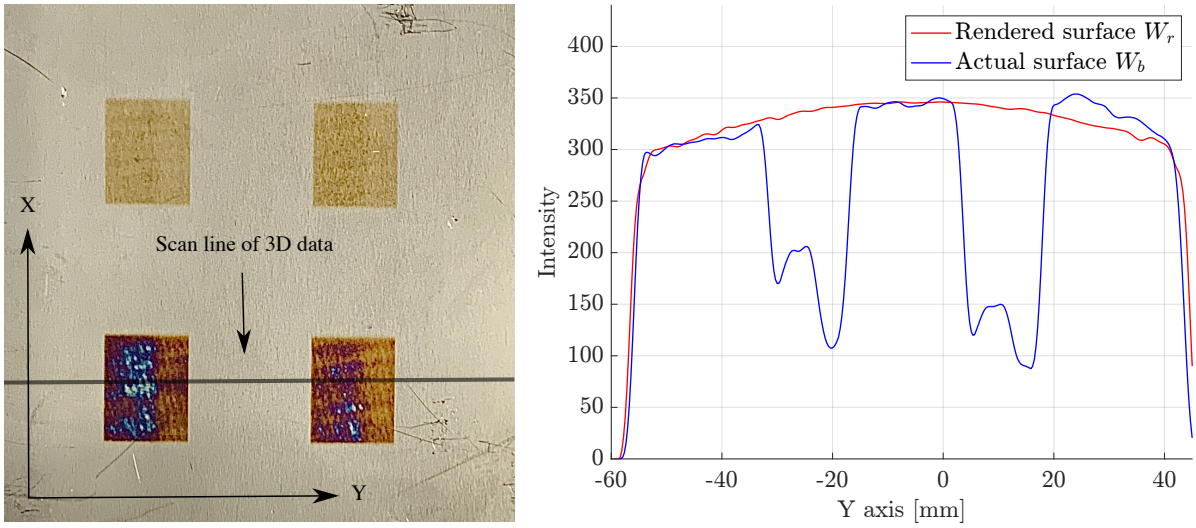

Figure 4. Left: A photograph of Sample 4 after laser marking. The different oxidation levels as a result of the induced heat are apparent. Right: A comparison of the rendered reference W_r and backscatter intensity W_b at a random scan line, indicated by the left figure. Note that the rendered surface follows the actual surface except for the oxidised areas as intended.

It can be observed from Figure 4 that the implemented model performs as intended. The rendered surface of W_r follows the actual surface W_b in the non-oxidised areas, which results in a relative change

in reflectivity ΔR, which approaches one. However, in the processed/oxidised areas, ΔR drops rapidly, which is expected as the surface colour has shifted into the red area as this in the opposite spectrum compared to the scanner laser's blue colour. It can further be observed from the rendered surface of Figure 4 that the highest intensity is not measured at the centre of the field of view. The slight shift away from the centre signifies that the sample is rotated at a small angle relative to the scanner, thus underlining the necessity of correcting the intensity for geometric effects.

From additional experiments, it was concluded that the ambient light has no substantial effect on the results. The method has also been tested at incident angles above 30°. Due to the specular nature of the measured surfaces, light is reflected away from the sensor, and the reflection could not be satisfactorily approximated. The proposed model was also able to render realistic surfaces for titanium, construction steel and aluminium. Though these samples were not laser marked, and thus any change in relative reflectivity was not approximated. Highly reflective or mirror-like surfaces are expected to be problematic, as the Cook-Torrance model is not well suited for such surfaces. In addition, the model is expected to be applicable for very rough surfaces that exhibit multi-reflections, assuming an isotropy random roughness as such surfaces will likely act as diffuse reflectors. Note that performing measurements simultaneously with active laser processing should be avoided, as processing light inevitably will be reflected into the CMOS sensor of the scanner, drastically influencing the results.

5. Conclusion

The study has examined the feasibility of applying a 3D scanner to measure backscatter intensities for determining surface absorption of stainless steel samples. The proposed solution is based on the Cook-Torrance BRDF to model the reflectance across the surface to generate a reference surface free of containments and oxidation. The generated reference surface is compared to the actual surface, acquired as backscatter intensity data from the 3D scanner. The ratio between the reference surface and the actual surface defines the relative change in reflectivity or absorption. The proposed solution was proven feasible as it could identify a change in the reflectivity locally across the surface when measuring an oxidised surface from laser marking.

Comparing the approximated change in reflectivity to those acquired by spectroscopy at the same wavelength (λ = 405 nm) showed a deviation of more than 70% in some cases. At the wavelength (λ = 1076 nm) of the processing laser, the deviation was more substantial, and thus an application of the proposed solution should be made using a measurement laser with a comparable wavelength. Part of the significant deviation could be attributed to noisy spectroscopy measurement. Research into establishing a mathematical relation between the approximated reflectance and the measured reflectance from spectroscopy could potentially improve the results.

The proposed solution shows significant potential for identifying areas with a potentially large change in absorption. In a production set-up, this knowledge could be applied to reject samples before processing. Providing a clean and homogenous surface for laser marking of samples and hence a better base for model verification could aid in defining the potential for the proposed solution. The results show that further work is necessary to improve the modelled accuracy and applicability of the model. This could include fitting a complete BRDF model to backscatter data acquired from a larger variation in scanning angles, thus making it possible to model the entire reflection into the hemisphere. In addition, introducing an anisotropic term to the model would add to the flexibility of the model.

Acknowledgements

The authors would like to acknowledge Peter Kjær Kristensen from Aalborg University for guiding the spectroscopy measurements. Innovation Fund Denmark, the INTERLASE project, with number 7050-00024B is gratefully acknowledged for supporting this project. The experimental equipment used for this project was supported by the Poul Due Jensen Foundation.

ORCID iDs
A F Mikkelstrup https://orcid.org/0000-0001-8209-6787
A N Thomsen https://orcid.org/0000-0003-4865-1032
M Kristiansen https://orcid.org/0000-0001-9652-3348

References

[1] Antończak A J, Stępak B, Kozioł P E and Abramski K M 2014 The influence of process parameters on the laser-induced coloring of titanium *Appl. Phys. A Mater. Sci. Process.* **115** 1003–13
[2] Dausinger F and Shen J 1993 Energy Coupling Efficiency in Laser Surface Treatment *ISIJ Int.* **33** 925–33
[3] Abedi H R and Hoseinpour Gollo M 2019 An experimental study of the effects of surface roughness and coating of Cr2O3 layer on the laser-forming process *Opt. Laser Technol.* **109** 336–47
[4] Niu C, Zhu T and Lv Y 2019 Influence of Surface Morphology on Absorptivity of Light-Absorbing Materials *Int. J. Photoenergy* **2019** 1-9
[5] Bergström D, Powell J and Kaplan A F H 2008 The absorption of light by rough metal surfaces-A three-dimensional ray-tracing analysis *J. Appl. Phys.* **103** 1–12
[6] Davim J P 2013 Laser Beam Manufacturing *Nontraditional Machining Processes* ed J P Davim (London: Springer London) chapter 2 pp 35-96
[7] Indhu R, Vivek V, Loganathan S, Bharatish A and Soundarapandian S 2018 Overview of Laser Absorptivity Measurement Techniques for Material Processing *Lasers Manuf. Mater. Process.* **5** 458–81
[8] Drude P 1900 Zur Elektronentheorie der Metalle *Ann. Phys.* **306** 566–613
[9] Hagen E and Rubens H 1903 Über Beziehungen des Reflexions- und Emissionsvermögens der Metalle zu ihrem elektrischen Leitvermögen *Ann. Phys.* **316** 873–901
[10] Ang L K, Lau Y Y, Gilgenbach R M and Spindler H L 1997 Analysis of laser absorption on a rough metal surface *Appl. Phys. Lett.* **70** 696–8
[11] Blidegn M S K and Olsen F O 1997 Investigation into the absorptivity change in metals with increased laser power *XI Int. Symp. Gas Flow Chem. Lasers High-Power Laser Conf.* **3092** 615-8
[12] Wang H, Kawahito Y, Yoshida R, Nakashima Y and Shiokawa K 2018 A model to calculate the laser absorption property of actual surface *Int. J. Heat Mass Transf.* **118** 562–9
[13] Wang J T, Weng C I, Chang J G and Hwang C C 2000 The influence of temperature and surface conditions on surface absorptivity in laser surface treatment *J. Appl. Phys.* **87** 3245–53
[14] Rubenchik A M, Wu S S Q, Kanz V K, LeBlanc M M, Lowdermilk W H, Rotter M D and Stanley J R 2014 Temperature-dependent 780-nm laser absorption by engineering grade aluminum, titanium, and steel alloy surfaces *Opt. Eng.* **53** 122506
[15] Bergström D 2008 *The absorption of laser light by rough metal surfaces* (Luleå University of Technology)
[16] Kügler H and Vollertsen F 2018 Determining Absorptivity Variations of Multiple Laser Beam Treatments of Stainless Steel Sheets *J. Manuf. Mater. Process.* **2** 84
[17] Vukašinovíc N, Bračun D, Možina J and Duhovnik J 2010 The influence of incident angle, object colour and distance on CNC laser scanning *Int. J. Adv. Manuf. Technol.* **50** 265–74
[18] Cook R L and Torrance K E 1982 A Reflectance Model for Computer Graphics *ACM Trans. Graph.* **1** 7–24
[19] Oren M and Nayar S K 1994 Generalization of Lambert's reflectance model *Proc. 21st Annu. Conf. Comput. Graph. Interact. Tech. SIGGRAPH 1994* 239–46
[20] Blinn J F 1977 Models of light reflection for computer synthesized pictures *Proc. 4th Annu. Conf. Comput. Graph. Interact. Tech. SIGGRAPH 1977* 192–8
[21] Johnson P B and Christy R W 1974 Optical constants of transition metals: Ti, V, Cr, Mn, Fe,

Co, Ni, and Pd *Phys. Rev. B* **9** 5056–70
[22] Schlick C 1994 An Inexpensive BRDF Model for Physically-based Rendering *Comput. Graph. Forum* **13** 233–46
[23] Walter B, Marschner S, Li H and Torrance K 2007 Microfacet models for refraction through rough surfaces *Eurographics* 195–206
[24] Heitz E 2014 Understanding the Masking-Shadowing Function in Microfacet-Based BRDFs *J. Comput. Graph. Tech.* **3** 48–107